Large Stroke Electrostatic Comb-Drive Actuators Enabled by a Novel Flexure Mechanism

Mohammad Olfatnia, Siddharth Sood, Jason J. Gorman, *Member, IEEE*, and Shorya Awtar, *Member, ASME*

***Abstract*—This paper presents in-plane electrostatic comb-drive actuators with stroke as large as 245 μm that is achieved by employing a novel clamped paired double parallelogram (C-DP-DP) flexure mechanism. The C-DP-DP flexure mechanism design offers high bearing direction stiffness K_x while maintaining low motion direction stiffness K_y over a large range of motion direction displacement. The resulting high (K_x/K_y) ratio mitigates the onset of sideways snap-in instability, thereby offering significantly greater actuation stroke compared with existing designs. Further improvement is achieved by reinforcing the individual beams in this flexure mechanism. While the traditional paired double parallelogram (DP-DP) flexure design with comb gap $G = 3$ μm and flexure beam length $L_1 = 1$ mm results in a 50-μm stroke before snap-in, the reinforced C-DP-DP design with the same comb gap and flexure beam length achieves a stroke of 141 μm. Furthermore, this C-DP-DP flexure design provides a 215-μm stroke with $G = 4$ μm and a 245-μm stroke with $G = 6$ μm. The presented work includes closed-form stiffness expressions for the reinforced C-DP-DP flexure, a design procedure for selecting dimensions of the overall comb-drive actuator, microfabrication of some representative actuators, and experimental measurements demonstrating the large stroke. [2012-0067]**

***Index Terms*—Comb drive, electrostatic actuator, flexure mechanism, large stroke.**

I. Introduction and Background

ELECTROSTATIC microelectromechanical systems (MEMS) comb-drive actuators have been used in various applications such as resonators [1], filters [2], microgrippers [3], [4], and micro/nano positioning [5], [6]. A linear in-plane electrostatic comb-drive actuator comprises two electrically isolated conductive combs with N fingers each, schematically shown in Fig. 1. While the static comb is fixed with respect to ground, the moving comb is guided via a flexure mechanism so that it can displace primarily in the $\mathbf{Y}$-direction with respect to the static comb. These static and moving comb fingers (length L_f, in-plane thickness T_f, and out-of-plane thickness H_f) have an interdigitation gap of G and an initial engagement of Y_o. The flexure mechanism is designed to provide linear guided motion and relatively small stiffness K_y in the $\mathbf{Y}$-direction (or motion direction), along with minimal error motions E_x and relatively high stiffness K_x in the $\mathbf{X}$-direction (or bearing direction). In an ideal scenario, K_y and E_x would approach zero while K_x would approach infinity. However, in practice, this is never the case given the performance tradeoffs between motion range, stiffness, and error motions that exist in flexure mechanisms [7], and manufacturing imperfections that are inherent to microfabrication processes [8], [9]. High stiffness K_θ and low error motion E_θ are also desirable in the in-plane yaw rotation [10]. Since K_θ can be independently made large and E_θ is inherently zero for the flexure designs considered here, in-plane rotation is initially ignored. The three out-of-plane directions are also bearing directions, but by appropriate choice of dimensions, become noncritical in the overall performance of the in-plane comb-drive actuator [11].

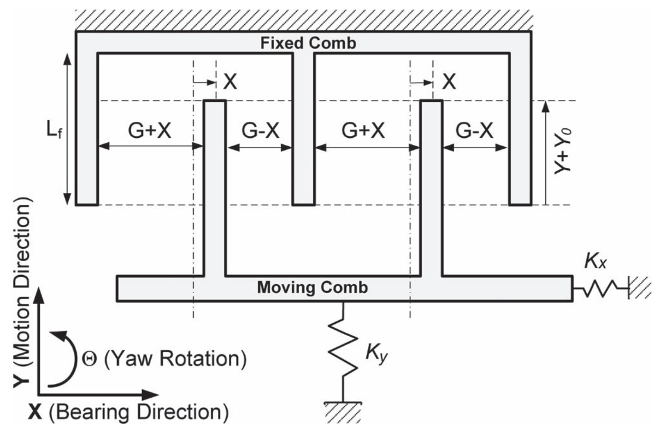

Fig. 1. Schematic of an electrostatic comb drive with the springs representing the flexure bearing.

When a voltage difference V is applied between the two combs, they experience an electrostatic attractive force, which displaces the moving comb by Y along the motion direction

$$K_y \cdot Y = \frac{\varepsilon N H_f G}{G^2 - X^2} V^2. \qquad (1)$$

Here, ε is the dielectric constant of air. Nonzero bearing direction displacement X can arise due to flexure error motion, fabrication misalignment, electrostatic forces, or a possible disturbance force in the $\mathbf{X}$-direction. While displacement Y is dictated by the comb geometry, motion direction flexure stiffness, and actuation voltage, its maximum stroke is limited by the snap-in phenomenon, which corresponds to sideways

Manuscript received March 15, 2012; revised October 19, 2012; accepted October 24, 2012. Date of publication December 12, 2012; date of current version March 29, 2013. This work was supported in part by the National Science Foundation under Grant CMMI-0846738. The work of S. Sood was supported by the National Institute of Science and Technology under a Measurement Science and Engineering Graduate Fellowship. The experimental portion of this work was performed at the Lurie Nanofabrication Facility, a member of the National Nanotechnology Infrastructure Network, which is supported in part by the National Science Foundation. Subject Editor L. Lin.

M. Olfatnia, S. Sood, and S. Awtar (corresponding author) are with the Department of Mechanical Engineering, University of Michigan, Ann Arbor, MI 48105 USA (e-mail: olfatnia@umich.edu; siddsood@umich.edu; awtar@umich.edu).

J. J. Gorman is with the Engineering Laboratory, National Institute of Standards and Technology, Gaithersburg, MD 20899 USA (e-mail: gorman@nist.gov).

Color versions of one or more of the figures in this paper are available online at http://ieeexplore.ieee.org.

Digital Object Identifier 10.1109/JMEMS.2012.2227458

instability of the moving comb [12], [13]. For any Y displacement, the electrostatic force due to the actuation voltage V produces a destabilizing or negative spring effect and the flexure mechanism offers a stabilizing or positive spring effect in the $\mathbf{X}$-direction. The former increases with increasing stroke, whereas the latter generally reduces. At the Y displacement when the former stiffness exceeds the latter, the moving comb snaps sideways into the static comb. This condition may be mathematically expressed as [12], [14]

$$\left(\frac{K_x}{K_y}\right) \leq \frac{2Y(Y+Y_0)}{G^2} \frac{\left(1+\frac{3X_c^2}{G^2}\right)}{\left(1-\frac{X_c^2}{G^2}\right)^2}, \text{ where } E_x = \frac{4X_c^3}{G^2+3X_c^2}. \quad (2)$$

This snap-in condition assumes that the comb fingers are perfectly rigid and all compliance comes from the flexure mechanism. Moreover, the yaw rotational stiffness K_θ of the flexure mechanism is assumed large enough to be ignored. The right-hand side represents a "critical stiffness ratio" needed to avoid snap-in and clearly increases with displacement Y and error motion E_x. E_x includes any motion or misalignment of the moving comb in the $\mathbf{X}$-direction with respect to its nominal zero position due to flexure mechanics or fabrication imperfections, in the absence of electrostatic force. Here, X_c is the actual $\mathbf{X}$-direction displacement at the onset of an electrostatic snap-in when an error or misalignment E_x is present. Clearly, to delay snap-in and maximize the actuator stroke, the flexure mechanism should provide a high (K_x/K_y) ratio and low E_x that are maintained over a large Y displacement range. Given the uncertainty in E_x from fabrication imperfections, its effect may be incorporated via a positive stability margin S. Stable operation is given by

$$\left(\frac{K_x}{K_y}\right) \geq \frac{2Y(Y+Y_0)}{G^2}(1+S),$$
$$\text{where } S = \left(1+\frac{3X_c^2}{G^2}\right) \Big/ \left(1-\frac{X_c^2}{G^2}\right)^2 - 1. \quad (3)$$

From (2), it can be shown that for an error motion that is 16% of the comb gap (e.g., $E_x = 0.64$ μm and $G = 4$ μm), a stability margin of 1 is required.

Large actuation stroke (> 100 μm) with limited footprint and actuation effort is desirable in a wide range of MEMS applications, including optical switches [12], data-storage systems [15], high-resolution microprinting [16], [17], endoscopic microscopy [18], neural microelectrodes [19], and scanning probe microscopy [5]. The broad goal of this paper is to investigate and overcome the fundamental limits in flexure mechanism design to maximize the stroke of MEMS comb-drive actuators while minimizing the device footprint and actuation voltage, for any given application. To meet this goal, we introduce a novel flexure mechanism, i.e., the clamped paired double parallelogram (C-DP-DP) flexure, shown in Fig. 2.

Section II provides a review of the prior art on flexure mechanism designs that have been traditionally used with comb-drive actuators and their limitations. The proposed C-DP-DP flexure mechanism, which offers a high (K_x/K_y) ratio over a large Y displacement range, is presented in Section III, along with closed-form analytical expressions for its stiffness. Section IV outlines a step-by-step recipe to optimally select the dimensions of this flexure mechanism and the comb drive to design an actuator with large stroke while minimizing actuation voltage and device footprint. Microfabrication of some representative actuators and experimental results are elaborated in Section V. Using the C-DP-DP flexure, a maximum actuation stroke of 245 μm with a 1-mm flexure beam length and a 6-μm comb gap is demonstrated.

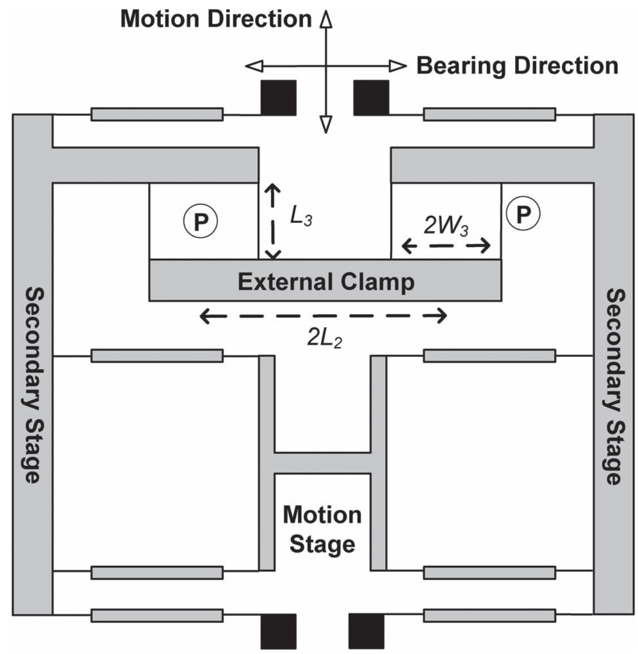

Fig. 2. Clamped paired double parallelogram (C-DP-DP) flexure.

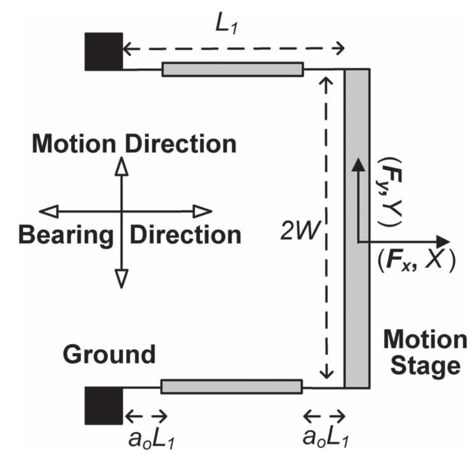

Fig. 3. Parallelogram (P) flexure.

II. Prior Art

Some of the earliest flexure designs used in comb-drive applications include the crab-leg flexure [13] and the folded-beam flexure [20], but both have limitations. While the former exhibits a K_y stiffness value that considerably grows with Y displacement, the latter provides a suboptimal K_x stiffness value that further deteriorates with increasing Y displacement [11].

The parallelogram (P) flexure, as shown in Fig. 3, is a common single-axis flexure mechanism and serves as an important building block in other flexure mechanisms that have been widely used in comb-drive actuators in the past and in the new flexure mechanism presented in this paper. Therefore, it is discussed in further detail here. In the P flexure shown in Fig. 3, a general shape is assumed for each constituent beam, with two equal end segments having uniform thickness T_1 and length $a_0 L_1$ and a rigid middle section of length $(1-2a_0)L_1$. Geometric parameter a_0 quantifies the degree of distributed compliance: $a_0 = 1/2$ represents a uniform thickness beam with highly distributed compliance, whereas smaller values of a_0 correspond to increasingly lumped compliance. In the subsequent discussion, a_0 serves as a geometric shape optimization parameter.

Closed-form nonlinear stiffness and error motion relations for this flexure have been previously derived [7] and are summarized here

$$K_y = \frac{2EI_1}{L_1^3} k_{11}^{(0)} \tag{4}$$

$$K_x = \frac{2EI_1}{L_1^3} \frac{k_{33}}{\left(1 + k_{33} g_{11}^{(1)} \left(\frac{Y}{L_1}\right)^2\right)} \tag{5}$$

$$K_\theta = \frac{2EI_1}{L_1^3} \cdot W^2 \cdot \frac{k_{33}}{\left(1 + k_{33} g_{11}^{(1)} \left(\frac{Y}{L_1}\right)^2\right)} \tag{6}$$

$$E_x = -\frac{k_{11}^{(1)}}{2} \frac{Y^2}{L_1} \tag{7}$$

$$E_\theta = \frac{k_{11}^{(0)}}{2W^2} \left(\frac{Y}{L_1}\right) \left(\frac{1}{k_{33}} + g_{11}^{(1)} \left(\frac{Y}{L_1}\right)^2\right). \tag{8}$$

Here, E is the Young's modulus of the material, and I_1 is the second moment of area $(= H_1 T_1^3/12)$. Nondimensional terms $k_{11}^{(0)}$, $k_{11}^{(1)}$, $g_{11}^{(1)}$, and k_{33} are all functions of the beam shape (a_o and T_1) and are referred to as beam characteristic coefficients [21]. These are graphically illustrated in Fig. 3 and mathematically expressed as follows:

$$\begin{aligned}
k_{11}^{(0)} &= \frac{6}{(3 - 6a_o + 4a_o^2)\, a_o} \\
k_{11}^{(1)} &= \frac{3\left(15 - 50a_o + 60a_o^2 - 24a_o^3\right)}{5\left(3 - 6a_o + 4a_o^2\right)^2} \\
g_{11}^{(1)} &= \frac{2a_o^3\left(105 - 630a_o + 1440a_o^2 - 1480a_o^3 + 576a_o^4\right)}{175\left(3 - 6a_o + 4a_o^2\right)^3} \\
k_{33} &= \frac{6}{a_0 (T_1/L_1)^2}.
\end{aligned} \tag{9}$$

Per (4), the P flexure provides low K_y stiffness that remains constant with Y and depends directly on coefficient $k_{11}^{(0)}$. $k_{11}^{(0)}$, which corresponds to the normalized elastic stiffness of an individual beam in the $\mathbf{Y}$-direction, is insensitive to values of a_0 around 0.5 but significantly grows as a_o decreases [see Fig. 4(b)]. Per (5), this flexure also provides high K_x stiffness at $Y = 0$, which depends on coefficient k_{33}. k_{33} is the nominal elastic stiffness of an individual beam in the $\mathbf{X}$-direction normalized with respect to its bending stiffness and also increases with reducing a_0 [see Fig. 4(a)].

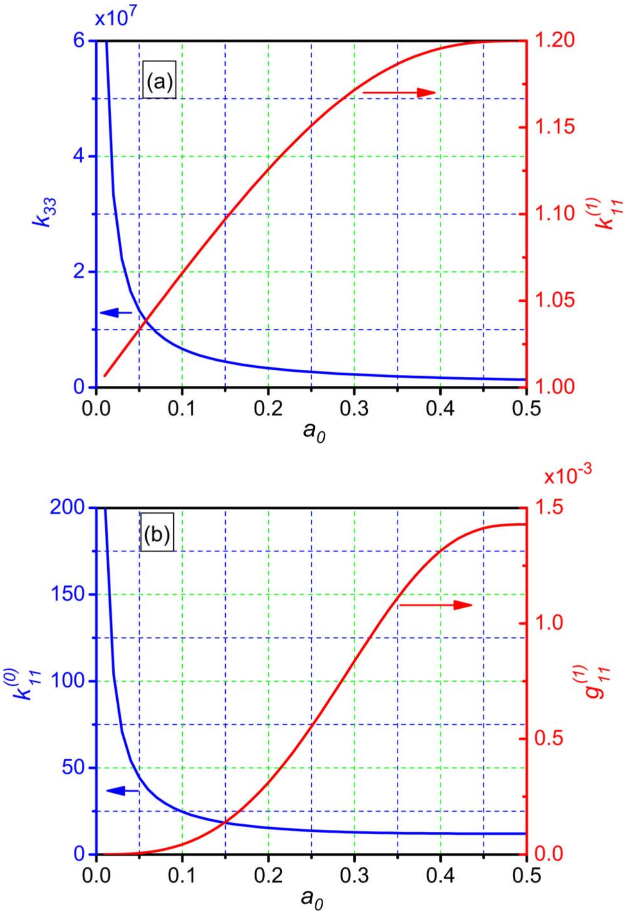

Fig. 4. Beam characteristic coefficients. For the k_{33} plot, (T_1/L_1) is assumed to be 0.003.

Furthermore, the stiffness K_x drops with increasing Y displacement due to the $k_{33} g_{11}^{(1)}$ term in the denominator of (5). Specifically, coefficient $g_{11}^{(1)}$ captures the elastokinematic effect in an individual beam that contributes additional $\mathbf{X}$-direction compliance in the presence of a Y displacement, and approaches zero with reducing a_0 [see Fig. 4(b)]. Since the product $k_{33} g_{11}^{(1)}$ also approaches zero with reducing a_0 (see Fig. 4), the drop in K_x stiffness can be reduced by decreasing a_0.

As given by (6), the rotational stiffness K_θ of this flexure mechanism follows a trend similar to K_x. However, the nominal value of this stiffness can be independently increased to be large enough by increasing the dimension W.

Thus, as evident in Fig. 6, the P flexure provides a favorable K_x/K_y stiffness ratio that can be further optimized by reducing a_o. However, the overwhelming disadvantage of this flexure mechanism is its large error motion E_x that arises due to the kinematics of beam arc-length conservation, which is captured via coefficient $k_{11}^{(1)}$. Since this kinematic coefficient is fundamental to the geometry of the beam, it always remains between 1 and 1.2, irrespective of the beam shape a_0, as evident in Fig. 4(a). The quadratic relation given by (7) shows that the motion stage in a P flexure follows a parabolic trajectory instead of a perfectly straight line. For typical beam dimensions ($L_1 = 1$ mm and $a_0 = 0.5$) and displacement $Y = 0.1L_1$, the E_x error motion is 6 μm, which is significant and would cause very early snap-in, as predicted by (2).

One effective method to alleviate this issue without eliminating E_x is to systematically prebend the beams of the P flexure, introduce an initial offset in the gap between the fixed and moving combs, and incline the comb fingers with respect to the Y-axis [22]. Grade *et al.* [23] implemented this clever idea to demonstrate a 175-μm comb-drive actuator stroke using $L_1 = 2$ mm and asymmetric comb gaps of 6 and 9 μm. While snap-in is thus mitigated, the trajectory of the motion stage is still parabolic, which can be undesirable in certain applications.

In order to eliminate the above E_x error motion, one might employ two P flexures in a symmetric parallel configuration (P-P) [24]. However, this results in an overconstrained geometry that produces a quadratic rise in the motion direction stiffness with increasing Y displacement and therefore a significantly restricted stroke. A more appropriate approach is to use two oppositely oriented P flexures in series. The resulting double parallelogram (DP) flexure employs the principle of geometric reversal to exactly cancel out the kinematic error motion of one P with that of the other P, in the absence of $\mathbf{X}$-direction force, to produce $E_x = 0$. Next, employing two DP flexures in parallel, as shown in Fig. 7, produces a symmetrical geometry that ensures $E_\theta = 0$ and reduced sensitivity to fabrication imperfections. In fact, the earliest reported comb-drive actuators employed the paired double parallelogram DP-DP flexure [1]. Subsequently, Legtenberg *et al.* [13] extensively studied this flexure for comb-drive actuation and reported a 39.9-μm stroke with $L_1 = 500$ μm and $G = 2.2$ μm.

Closed-form nonlinear stiffness relations for the DP-DP flexure have been also previously derived [7] and are summarized here

$$K_y = \frac{2EI_1}{L_1^3} k_{11}^{(0)} \tag{10}$$

$$K_x = \frac{2EI_1}{L_1^3} \frac{k_{33}}{\left(1 + k_{33}\left(g_{11}^{(1)} + \frac{\left(k_{11}^{(1)}\right)^2}{k_{11}^{(0)}}\right)\left(\frac{Y}{2L_1}\right)^2\right)} \tag{11}$$

$$K_\theta = \frac{EI_1}{L_1^3} \cdot \frac{4W_1^2 W_2^2}{(W_1^2 + W_2^2)} \cdot \frac{k_{33}}{\left(1 + k_{33} g_{11}^{(1)} \left(\frac{Y}{2L_1}\right)^2\right)}. \tag{12}$$

The motion direction stiffness K_y of the DP-DP flexure is low and remains largely invariant with Y displacement, i.e., same as that of the P flexure. However, while its nominal K_x stiffness at $Y = 0$ is the same as that of the P flexure, the drop in K_x with increasing Y displacement is far more precipitous. The reason being that, in addition to the $k_{33} g_{11}^{(1)}$ term in the denominator of (11), there is now a new term, i.e., $(k_{11}^{(1)})^2 k_{33}/k_{11}^{(0)}$, which is at least two orders of magnitude greater than the former. Since this term is dependent on kinematic coefficient $k_{11}^{(1)}$, it is largely insensitive to variations in a_0 and never approaches zero (see Fig. 5). Therefore, while the nominal K_x/K_y ratio at $Y = 0$ for a DP-DP flexure can be increased by employing a lower value of a_o, the steep decline in this stiffness ratio remains unaffected by beam shape variation (see Fig. 6). In this figure, a representative critical stiffness ratio curve for a typical comb-drive actuator demonstrates how the narrow profile of the K_x/K_y ratio versus Y displacement produces an early snap-in and limited stroke when the DP-DP flexure is used.

It is noteworthy that the in-plane rotational stiffness K_θ in this case, given by (12), follows a trend very similar to the P

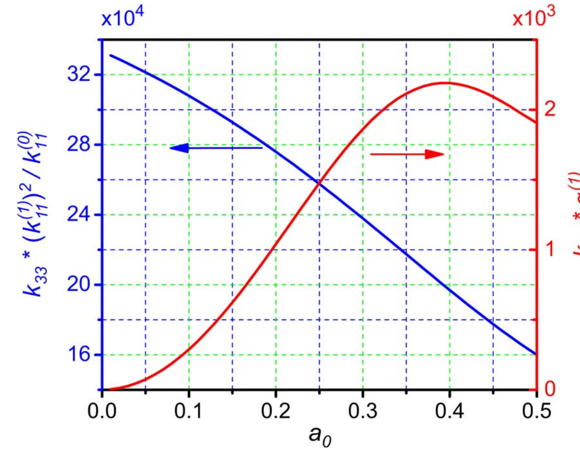

Fig. 5. Elastokinematic and kinematic contributions to the bearing direction compliance of the P and DP-DP flexures.

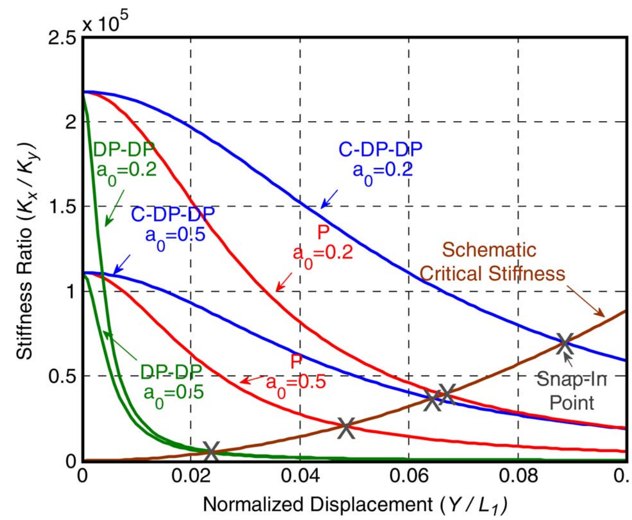

Fig. 6. (K_x/K_y) stiffness ratio provided by the P, DP-DP, and C-DP-DP flexures for different values of beam reinforcement a_o. A representative critical stiffness curve is included to demonstrate the effect of stiffness ratio on comb-drive actuator snap-in.

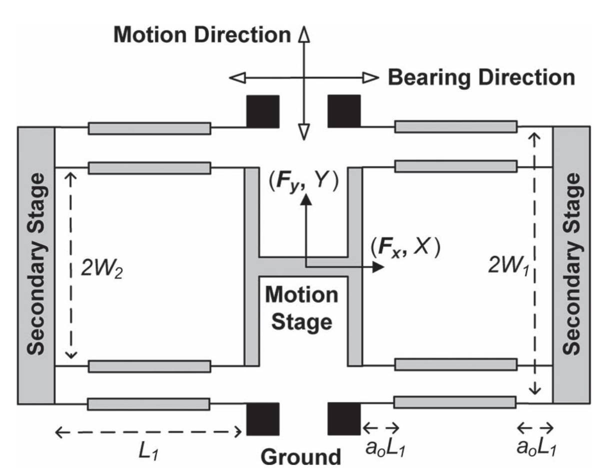

Fig. 7. Paired double parallelogram (DP-DP) flexure.

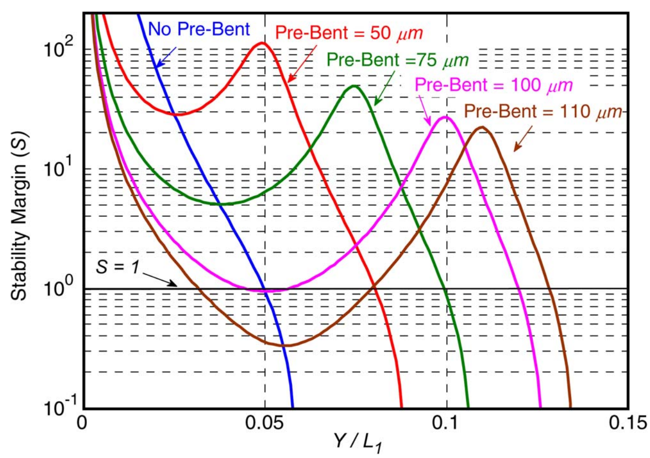

Fig. 8. Degradation in the stability margin with increasing beam prebend in DP-DP flexures.

flexure. As a result, the drop in K_θ stiffness from its nominal value with increasing Y displacement is far more gradual. In addition, this stiffness can be independently made large by appropriate choice of the dimensions W_1 and W_2.

Recognizing the limitation of this narrow K_x/K_y stiffness ratio profile and the fact that its maximum value occurs at $Y = 0$ where the required critical stiffness ratio is minimum, DP and DP-DP flexures with prebent [25] or pretilted [26] beams have been used to improve the comb-drive actuator stroke. Appropriately prebent beams shift the Y displacement value at which K_x is maximum, without abating the drop in K_x or affecting K_y [12]. Thus, by providing a greater K_x/K_y stiffness ratio at larger displacements, where it is most needed, prebending provides improvement in the actuator stroke. With 500-μm beam length, 30-μm pretilt, and 2-μm comb gap, Zhou and Dowd [26] reported a 61-μm stroke, which was two times higher compared with a similar DP-DP flexure without any pretilt. Grade *et al.* [12] also reported strokes as high as 150 μm with a 1.1-mm beam length, approximately 100-μm prebend, and 8.5-μm comb gap. However, these improvements in stroke come at the expense of robustness [14], as illustrated in Fig. 8.

For a given set of DP-DP dimensions, greater prebending causes the stability margin S to fall to levels below 1 over the expected actuator stroke. This makes the design vulnerable to premature snap-in, given the presence of finite fabrication imperfections. It can be shown that, to keep S greater than 1 over the actuation stroke, the maximum prebend in a DP or DP-DP flexure should be less than

$$Y_{P-B-\max} \approx \sqrt{\frac{4GL_1}{k_{11}^{(1)}}}. \tag{13}$$

Here, $Y_{P-B-\max}$ represents the overall shift in the K_y stiffness peak along the Y displacement axis due to prebending of beams. For the typical values of $L_1 = 1$ mm, $G = 3$ μm, and $a_0 = 0.5$, the maximum allowable prebend is 100 μm, as shown in Fig. 8.

Thus, in the flexure designs considered in the literature so far, there exist clear performance tradeoffs between stiffness, error motions, and robustness, which affect their ability to provide very large strokes in comb-drive actuators. The desirable goal in a flexure mechanism design is to ensure inherently low error motions, achieve a high nominal value of the K_x/K_y ratio, and prevent the steep decline of this stiffness ratio with increasing Y displacement. As shown in Fig. 5, these stiffness goals are accomplished via the new C-DP-DP flexure design presented in this paper.

However, before describing the C-DP-DP flexure design in the next section, it is important to first physically understand the source of the steep decline in K_x seen in the DP and DP-DP mechanisms, as well as their prebent versions. As noted earlier, the kinematic effect associated with arc-length conservation is fundamental to a beam flexure and does not go away simply by beam shape optimization. It also produces a load-stiffening effect in each beam flexure that linearly increases the $\mathbf{Y}$-direction stiffness in the presence of an $\mathbf{X}$-direction force. The reason these kinematic and load-stiffening effects play an important role in the DP-DP flexure's K_x stiffness is because of the mechanism's topology. In this design, the secondary stages of both DPs are inadequately constrained in the $\mathbf{Y}$-direction. As a consequence, when the Y displacement of the motion stage is held fixed and a small bearing direction force $\boldsymbol{F}_x$ is applied, the two secondary stages move opposite to each other in the motion direction from their nominal displacement of $Y/2$. This is because the $\mathbf{Y}$-direction stiffness of each of the P flexures within the two DPs changes in the presence of $\boldsymbol{F}_x$ due to the above load-stiffening effect. In the presence of this "extra" $\mathbf{Y}$-direction displacement of the two secondary stages, the kinematic errors of the individual P flexures in the $\mathbf{X}$-direction no longer cancel out perfectly, thereby producing an "extra" X displacement at the motion stage and therefore lower K_x.

Thus, the above-described steep decline in K_x can be restricted by appropriately constraining the $\mathbf{Y}$-direction displacement of both secondary stages such that they always remain at their nominal value of $Y/2$, i.e., at half that of the motion stage. This was recognized several decades ago in the context of precision motion guidance instruments, and an external-lever-based solution was proposed [27]. A lever arm was employed to kinematically enforce a 1:2 ratio between the $\mathbf{Y}$-direction displacements of the secondary stage and the motion stage in a DP flexure. A microfabricated variation of this design has been used by Brouwer *et al.* [28] to successfully restrict the drop in K_x stiffness and improve the comb-drive actuation stroke. They reported a 100-μm stroke with a 1-mm beam length and a 4-μm comb gap. However, certain challenges remain with this design. The use of an external lever increases motion direction stiffness K_y, which is detrimental to the K_x/K_y ratio and increases actuation effort. In addition, this design limits access to the motion stage and increases the overall device footprint, as compared with the basic DP flexure.

Apart from the flexure mechanism design, several other techniques have been also investigated and employed to increase the stroke of comb-drive actuators. These include shape optimization of the comb fingers [29], [30], varying comb-finger lengths [12] within a comb, multiple comb sets that are sequentially powered [31], [32], and flexure-based displacement amplifiers [33]–[36]. While these techniques have their respective pros

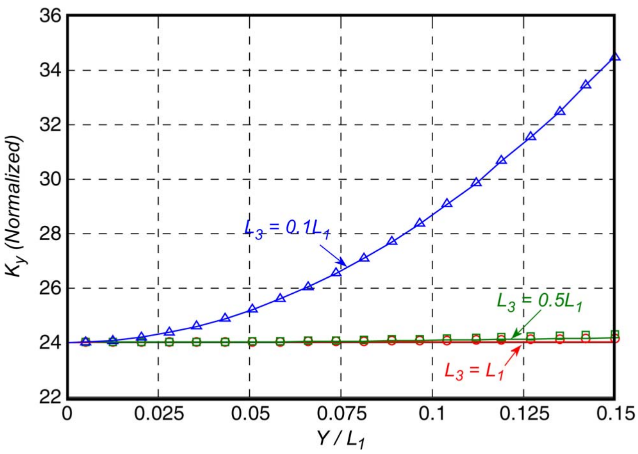

Fig. 9. Motion direction stiffness for different values of L_3 in the C-DP-DP flexure [(solid line) closed-form analysis; (markers) FEA]. K_y stiffness is normalized with respect to EI_1/L_1^3.

and cons, they are peripheral to the present discussion and therefore not considered in further detail here.

III. Proposed Design

To achieve the desired stiffness and error motion goals, our strategy is to work with the DP-DP flexure but constrain its secondary stages in a unique manner. In the proposed C-DP-DP flexure mechanism [37], as shown in Fig. 2, the two secondary stages are connected to an external clamp via secondary P flexures. The high rotational stiffness of these P flexures minimizes any relative Y displacement between the two secondary stages, forcing them to maintain $Y/2$ displacement at all times. This constrains these stages from responding to an $\mathbf{X}$-direction force on the motion stage. In addition, the low $\mathbf{X}$-direction stiffness of the secondary P flexures offers minimal resistance to the kinematic $\mathbf{X}$-direction displacement of the secondary stages. The analytical relations for the motion and bearing stiffness of the C-DP-DP flexure have been separately derived [38] and are summarized here

$$K_y = \frac{EI_1}{L_1^3}\left(2k_{11}^{(0)} + \frac{9k_{11}^{(0)}k_{11}^{(1)}}{20}\left(\frac{L_1^3}{L_3^3}\right)\left(\frac{Y}{L_1}\right)^2\right) \tag{14}$$

$$K_x = \frac{EI_1}{L_1^3}\frac{2k_{33}}{\left(1 + k_{33}\left(g_{11}^{(1)} + \frac{\left(k_{11}^{(1)}\right)^2}{k_{11}^{(0)}(1+\eta)}\right)\left(\frac{Y}{2L_1}\right)^2\right)} \tag{15}$$

$$\text{where } \eta = \left(\frac{6W_3^2L_1^3}{k_{11}^{(0)}L_2^2L_3T_3^2}\right).$$

The beam characteristic coefficients here are the same as earlier [see (9)]. Although beams in the secondary parallelograms are assumed to be of uniform thickness (i.e., $a_o = 0.5$), it is straightforward to introduce a separate beam shape parameter for them, if needed.

Equation (14) shows that there is a slight increase in K_y because of the external clamp. However, this can be mitigated by choosing a large-enough secondary parallelogram beam length L_3 (see Fig. 9). Next, the effectiveness of the clamp in restricting the precipitous drop in the bearing direction stiffness K_x is captured via the dimensionless parameter η in (15). The

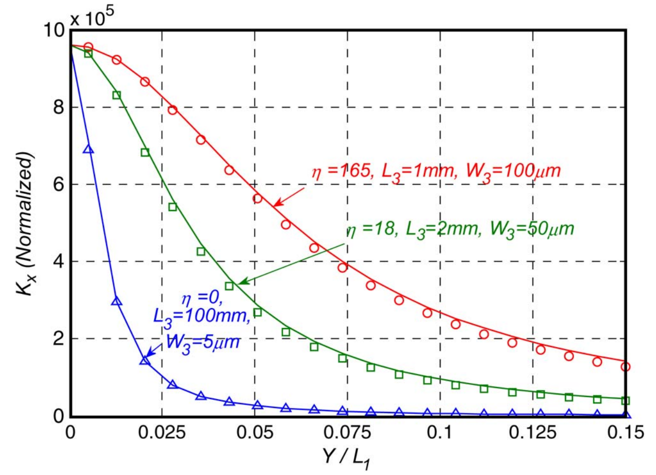

Fig. 10. Bearing direction stiffness for different values of η in the C-DP-DP flexure [(solid line) closed-form analysis; (markers) FEA]. K_x stiffness is normalized with respect to EI_1/L_1^3.

external clamp prevents relative Y motion between the two secondary stages by employing the high rotational stiffness of its constituent parallelograms, which manifests itself in the form of η. For low values of W_3, this stiffness and therefore η are small. It may be analytically seen that as $\eta \rightarrow 0$, the K_x stiffness becomes exactly the same as that for a DP-DP flexure, which corresponds to a completely ineffective clamp (see Fig. 10). However, as W_3 increases, parameter η also increases. Equation (15) shows that as η becomes very large, the kinematic term $(k_{11}^{(1)})^2/k_{11}^{(0)}$ vanishes and only the elastokinematic term $g_{11}^{(1)}$ remains. Since the latter is at least two orders of magnitude smaller than the former, this implies that the drop in K_x stiffness now is significantly reduced and that the clamp proves to be effective. Furthermore, because of the sensitivity of the elastokinematic term to beam shape, reinforced beams $(a_0 < 0.5)$ may be used to produce even greater improvements in the bearing stiffness K_x of the C-DP-DP flexure (see Fig. 6). This is in contrast with the DP-DP flexure for which beam reinforcement produces marginal benefits.

The (K_x/K_y) stiffness ratio of the C-DP-DP flexure for two different values of a_o is shown in Fig. 6, which demonstrates its superior stiffness characteristics compared with the DP-DP and P flexures. Moreover, unlike the P flexure, the C-DP-DP flexure provides inherently zero E_x and E_θ error motions. Because of these attributes, it is evident in Fig. 6 that the C-DP-DP is capable of producing very large strokes in comb-drive actuators.

The in-plane yaw stiffness K_θ of a C-DP-DP flexure with high η remains the same as that for the DP-DP, as given by (12). As aforementioned, this stiffness can be independently made large by appropriate choice of the dimensions W_1 and W_2 such that it does not affect the snap-in condition and therefore the actuation stroke.

All the closed-form analytical results in this section assume perfectly rigid stages, external clamp, ground anchors, and beam reinforcements. These results have been also validated via nonlinear finite-elements analysis (FEA). A comparison between the closed-form and FEA results is presented in Figs. 9 and 10 for the normalized K_y and K_x stiffness values, respectively.

The following dimensions were used to generate the results plotted in these figures: $L_1 = 1$ mm, $T_1 = 5$ μm, $W_1 = 250$ μm, $W_2 = 400$ μm, $L_2 = 1.1$ mm, $a_0 = 0.5$, and $H_1 = 50$ μm; $W_3 = 250$ μm, and L_3 varies in Fig. 9; both L_3 and W_3 vary in Fig. 10.

IV. Comb-Drive Actuator Design Recipe

In this section, we present a systematic procedure for designing a C-DP-DP flexure-based comb-drive actuator to maximize its actuation stroke while minimizing device footprint and actuation voltage. In an actual application, one would take into account any additional constraints imposed by that application in addition to the procedure and steps presented here.

Given the several constraints and tradeoffs involved, the goal here is to obtain a good starting point for the flexure and comb-drive dimensions (i.e., L_1, T_1, a_0, W_1, W_2, L_2, L_3, W_3, G, L_f, and T_f) based on some simplifying assumptions and subsequently iterate to further refine the overall design.

The following assumptions are initially made and are revisited during later design steps.

1) Analytical results in the previous section show that the optimization of the external clamp and secondary parallelograms is decoupled from the final stiffness of the C-DP-DP flexure, as long as the clamp is effective. Since an optimal clamp that provides high η can always be created subsequently, motion and bearing stiffness values corresponding to high $\eta(\rightarrow \infty)$ are assumed at the onset of this design procedure, i.e.,

$$K_y = \frac{2EI_1 k_{11}^{(0)}}{L_1^3} \tag{16}$$

$$K_x = \frac{2EI_1}{L_1^3} \frac{k_{33}}{\left(1 + k_{33} g_{11}^{(1)} \left(\frac{Y}{2L_1}\right)^2\right)}. \tag{17}$$

2) The motion stage, secondary stage, external clamp, ground anchors, and beam reinforcements are all assumed to be perfectly rigid.
3) Since the in-plane rotational stiffness K_θ of the C-DP-DP flexure can be made independently high, it is assumed large enough to be ignored in the first iteration.
4) Although the C-DP-DP flexure exhibits theoretically zero error motions in the $\mathbf{X}$- and $\mathbf{\Theta}$-directions because of its inherent symmetry, misalignment and error motions due to fabrication imperfection are inevitable. Therefore, a stability margin of $S = 1$ is assumed to provide robustness against such nondeterministic factors. This may have to be revised in subsequent iterations.
5) Silicon is chosen as the flexure and comb-drive material, which sets an upper bound for the maximum achievable stroke due to mechanical failure. For the C-DP-DP flexure, the yield limit is given by [7]

$$Y_{\text{yield}} \leq \left(\frac{8}{k_{11}^{(0)}}\right) \left(\frac{S_y}{E}\right) \left(\frac{L_1^2}{T_1}\right) \tag{18}$$

where S_y is the material yield strength.

6) An initial comb-finger engagement Y_0 is needed to overcome fringing effects that are important for small Y displacements. However, Y_0 is much smaller than the maximum Y displacement and is therefore initially dropped in the design procedure.

With these assumptions, one can now substitute the motion and bearing direction stiffness expressions for an optimal C-DP-DP [see (16) and (17)] into the snap-in condition (3) for a comb-drive actuator

$$\frac{k_{33}}{k_{11}^{(0)} \left(1 + k_{33} g_{11}^{(1)} \left(\frac{Y_{\max}}{2L_1}\right)^2\right)} = \frac{4Y_{\max}^2}{G^2}. \tag{19}$$

This snap-in condition corresponds to maximum motion direction displacement $Y_{\max}$, which is also the actuation stroke, and associated stiffness values. The actuation voltage $V_{\max}$ at this maximum displacement may be obtained from (1), i.e.,

$$NV_{\max}^2 = \frac{E}{6} \left(\frac{T_1}{L_1}\right)^3 \frac{k_{11}^{(0)} Y_{\max} G}{\varepsilon}. \tag{20}$$

The left-hand side in the above equation represents the actuation effort, which should generally be minimized. Lower N helps reduce the device footprint, and $V_{\max}$ is often restricted by practical instrumentation and operational limits.

As aforementioned, $k_{11}^{(0)}$, $g_{11}^{(1)}$, and k_{33} are all functions of a_o and (T_1/L_1), as given by (9). We next present a step-by-step recipe for choosing the dimensions of the C-DP-DP and comb drive that employs the analytical knowledge compiled so far.

Step 1: Start with assuming a dimension for the flexure beam length L_1, which directly impacts the device footprint. In the first iteration, we choose an initial L_1 value of 1 mm.

Step 2: Minimizing the T_1/L_1 ratio lowers the actuation effort [see (20)] and reduces the bending stress in the flexure beams. A smaller T_1/L_1 ratio also increases the left-hand side of (19), thus delaying the snap-in condition. Therefore, the flexure beam thickness should be chosen to be a small value dictated by the practical limits of the microfabrication process. As mentioned in the next section, this limit is 1.7 μm in our case, and with an adequate safety margin, we choose $T_1 = 3$ μm, which corresponds to a T_1/L_1 ratio of 0.003.

Step 3: Now, the two key remaining design variables in (19) and (20) are a_0 and G. These two equations may be simultaneously solved to eliminate G to produce:

$$NV_{\max}^2 = \frac{E}{3\varepsilon} \left(\frac{T_1}{L_1}\right)^3 Y_{\max}^2 \sqrt{\left(k_{11}^{(0)}\right)^3 \left[\frac{1}{k_{33}} + \left(\frac{Y_{\max}}{2L}\right)^2 g_{11}^{(1)}\right]}. \tag{21}$$

The above condition can be plotted on an $NV_{\max}^2$ versus $Y_{\max}$ graph for multiple fixed values of a_0 (see Fig. 11). Each solid line, referred to an iso$-a_0$ line, represents a fixed value of a_0 and varying values of G. Similarly, the above equations are solved to eliminate a_o, and the resulting condition is plotted on the same $NV_{\max}^2$ versus $Y_{\max}$ graph for fixed values of G. Each dashed line, referred to an iso$-G$ line, represents a fixed value of G and varying values of a_0. Moving along an iso$-a_0$ line, it is clear that for a given beam shape a_0, one can achieve higher stroke by increasing the comb gap G, but this also increases

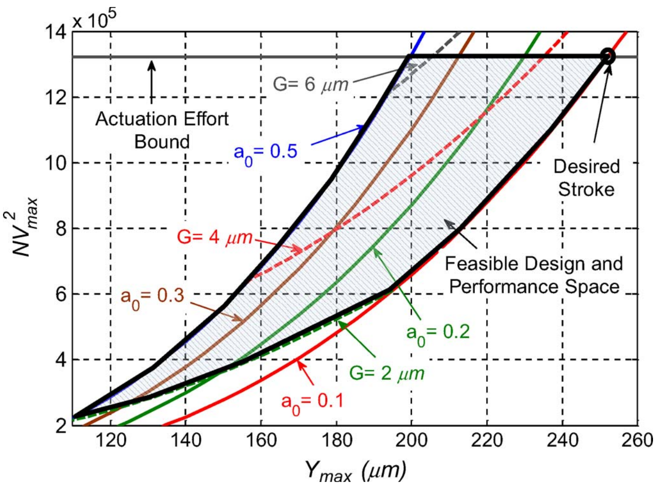

Fig. 11. Design and performance space for C-DP-DP flexure-based comb-drive actuators.

the actuation effort $NV_{\max}^2$. Similarly, moving along an iso$-G$ line, one can achieve greater stroke by reducing a_0, which once again leads to a higher actuation effort.

From the design and performance space presented in Fig. 11, one can graphically choose the beam shape a_0 and comb gap G to maximize stroke while minimizing the actuation effort. There is a lower bound on G dictated by the microfabrication process (2 μm, in our case) and an obvious upper bound on a_0 (0.5). These bounds produce a feasible design and performance space, indicated by the shaded region in Fig. 11.

Step 4: At this point, one can either set a maximum allowable actuation effort and pick the corresponding actuation stroke or alternatively choose the desired actuation stroke and pick the actuation effort. We choose a desired actuation stroke greater than or equal to 250 μm.

Step 5: For a desired stroke, clearly, smaller values of a_o and G in the feasible design space result in the lowest actuation effort. However, one has to be cautious while choosing small values of these two design variables. Small a_o leads to increasingly higher stresses in the flexure beams, and the material failure becomes a concern. For a given $Y_{\max}$, a_0 may be chosen to maintain an adequate margin of safety against material failure using (18). Separately, the snap-in condition becomes highly sensitive to error motions E_x for very small G, and the assumed safety margin S of 1 can prove to be inadequate. For our final designs, we chose $a_0 = 0.2$ and G values in the range of 3 μm to 6 μm.

Step 6: Having chosen a_o and G in the previous step, we now have a numerical value of the actuation effort from Fig. 11. The number of comb fingers N can be chosen next while keeping the maximum actuation voltage $V_{\max}$ within relevant practical limits. We selected $V_{\max} = 150$ V based on our existing instrumentation capabilities.

Step 7: One can now start to lay out the flexure mechanism and the comb drive. The dimensions W_1 and W_2 should be chosen such that rotational stiffness K_θ given by (12) is adequately high. If it is more than an order of magnitude higher than $K_x L_4^2$ at $Y_{\max}$, the contribution of the rotational stiffness can be entirely ignored. Here, L_4 is the distance along the Y-axis from the center of the flexure mechanism to the tip of the comb fingers. If this condition is not met, then the rotational stiffness should be taken into account in the next iteration using a modified version of the snap-in condition [10]. The ratio γ between the reduced actuation stroke due to finite rotational stiffness and the predicted stroke assuming infinite rotational stiffness is graphically illustrated for two values of a_0 in Fig. 12.

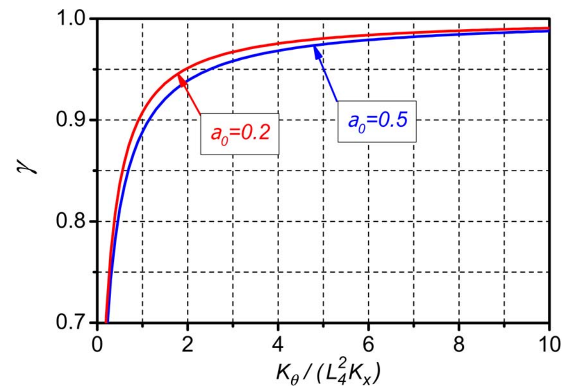

Fig. 12. Reduction in predicted actuation stroke in the presence of finite rotational stiffness.

Step 8: The external clamp is designed next. Using (14), choose L_3 to be large enough so that the increase in the motion direction stiffness K_y due to the clamp over the above-selected $Y_{\max}$ is within a few percent (i.e., 5%, in our designs). Next, choose T_3 to be a small but practically feasible value. We choose T_3 to be equal to T_1. Next, choose W_3 and L_2 to make the clamp effectiveness parameter η at least 100. With an effective clamp thus designed, it can now be included in the overall device layout.

Step 9: Next, choose the in-plane thickness of the reinforced beam section to be at least five times the thickness of the end segment T_1, which ensures more than 125 times bending stiffness. Furthermore, choose the in-plane thickness for the motion stage, secondary stages, and external clamp to be at least 40 times T_1. If these dimensions are chosen to be less for whatever reason, then the contribution of these stages to the bearing direction stiffness K_x should be estimated, and a revised snap-in condition with this reduced effective K_x should be used in the next design iteration.

Step 10: Choose Y_0 to be at least two to three times the comb gap G [39]. Then, choose the comb-finger length L_f to be slightly greater than $(Y_0 + Y_{\max})$. For this comb-finger length, the comb-finger thickness T_f should be chosen to avoid local snap-in of individual fingers. This is given by the following condition [40]:

$$T_f \geq \left(2\frac{\varepsilon L_f^4}{EG^3}V_{\max}^2\right)^{\frac{1}{3}}. \tag{22}$$

A margin of safety may be included (i.e., 1.5, in our case) while using the above relation.

Step 11: The depth of the flexure beams and comb fingers, i.e., H_f, does not play a role in the overall actuator performance and should be selected to be large enough to avoid out-of-plane collapse during fabrication or operation.

TABLE I

COMB-DRIVE ACTUATORS THAT WERE DESIGNED, FABRICATED, AND TESTED. ALL LENGTH DIMENSIONS ARE IN MICROMETERS

Flexure Design	G	T_f	N	L_f	T_1	L_1	L_2	L_3	W_1	W_2	W_3	H_1	a_0	*Predicted/Designed Stroke*			*Measured Stroke*	*Voltage at Stroke (V)*
														S=0	*S=1*	*S=1.5*		
DP-DP	3	6	50	150	4	1000	--	--	400	250	--	50	0.5	59	50	47	50	85
C-DP-DP	3	9	80	210	4	1000	1000	430	790	250	240	50	0.2	228	191	181	141	95
C-DP-DP	3	7	80	180	4	1000	1000	430	790	250	240	50	0.5	164	138	130	119	90
C-DP-DP	4	8	70	240	3	1000	1000	430	810	250	240	50	0.2	272	230	218	215	104
C-DP-DP	4	7	70	210	3	1000	1000	430	790	250	240	50	0.3	224	188	178	170	91
C-DP-DP	4	7	70	190	3	1000	1000	430	780	250	240	50	0.4	202	169	160	157	91
C-DP-DP	6	8	100	290	3	1000	1500	430	875	300	360	50	0.2	341	287	271	245	119

This concludes the first iteration of the overall actuator's dimensional layout, including the flexure and the comb drive. If the device footprint turns out to be too large or too small, one can start the process again from Step 1 with a different value of beam length L_1. Once an acceptable footprint is achieved, a final check on the actuation, snap-in, and material failure conditions should be performed while removing the previously listed assumptions. Specifically, the choice of stability margin S should be dictated by the selected comb-gap value G and the accuracy of the microfabrication process used. Accordingly, a higher value of S may be used in subsequent iterations. These iterations can lead to further refinement of the flexure and comb-drive dimensions.

This procedure was used to design several devices that were then fabricated and tested. Young's modulus value of 165 GPa (corrected by 3% for P-type doping), as reported in the literature [41], was assumed. Table I summarizes the dimensional details of the designs that were fabricated, and their testing is discussed in the next section.

Finally, if the comb-drive actuator is designed for an application that requires additional force capability at the motion stage (or shuttle), then the actuation and stability conditions (1) and (2) slightly change. Specifically, the desired additional force should be added to the left-hand side of the $\mathbf{Y}$-direction force equilibrium [see (1)]. The rest of the design process can be calibrated and carried out in a manner analogous to the one described above.

V. EXPERIMENTAL RESULTS AND DISCUSSION

A. Fabrication

The comb-drive actuators were fabricated using silicon-on-insulator wafers with a device layer of 50 μm, a buried oxide layer of 2 μm, and a silicon handle layer of 350 μm. The device layer is heavily boron doped (P-type) with resistivity less than 0.01 $\Omega \cdot$ cm. The silicon handle layer was first patterned and etched by deep reactive-ion etching (DRIE), and then the buried oxide was removed by HF (49%). Finally, the device layer was patterned and etched by DRIE. After the last etching process, critical point drying was used to dry the samples to avoid stiction [42]. In this drying method, liquid CO_2 is transferred to vapor via the supercritical phase (at $T_c = 38°, P_c = 80$ atm) to avoid capillary forces that arise from the surface tension at the liquid–vapor interface. A scanning electron microscope (SEM) image of a representative fabricated device is shown in Fig. 13.

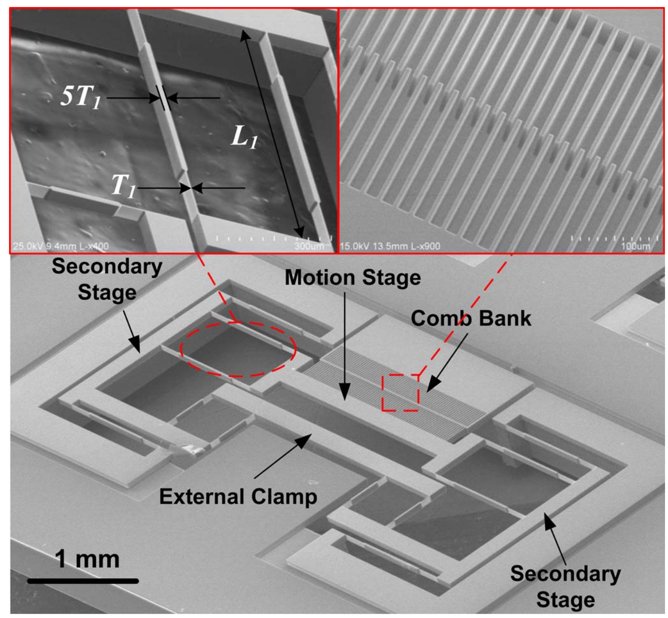

Fig. 13. SEM image of a microfabricated comb-drive actuator employing the C-DP-DP flexure.

B. Characterization

The fabricated comb-drive actuators were driven by a dc voltage source using electrical probes applied to the fixed and moving combs. The voltage was swept from zero to the maximum voltage at snap-in in a ramp profile with 1-V increments. The displacement response of the actuators was observed with a microscope and captured by a charge-coupled-device camera. Subsequently, the displacement of the actuators was quantitatively measured using image-processing software. The Y displacement measurements were found to be repeatable within 1 μm.

C. Voltage–Stroke Curves

Fig. 14 demonstrates the displacement versus voltage curves for three different flexure designs, each with a comb gap of 3 μm, a beam length of 1 mm, and a beam thickness of 4 μm. The figure shows theoretical predictions and experimental measurements. The measured stroke of a conventional DP-DP flexure with these dimensions and $a_0 = 0.5$ was 50 μm. Referring to Table I, this indicates that $S = 1$ is a reasonable stability margin to use for the DP-DP flexure and the microfabrication process described above. The measured

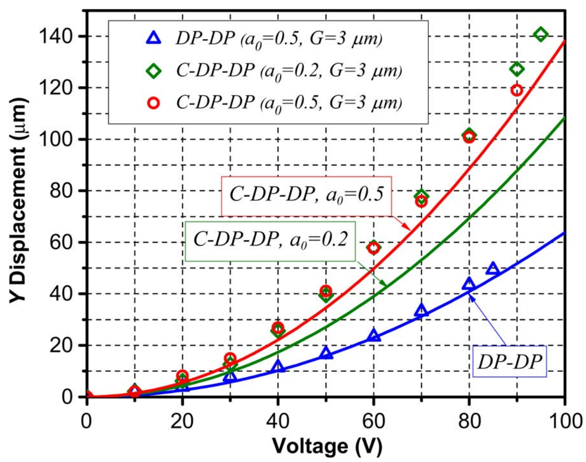

Fig. 14. Y displacement versus voltage for DP-DP and C-DP-DP flexure-based comb-drive actuators [*(solid lines) theoretical; (markers) experimental*].

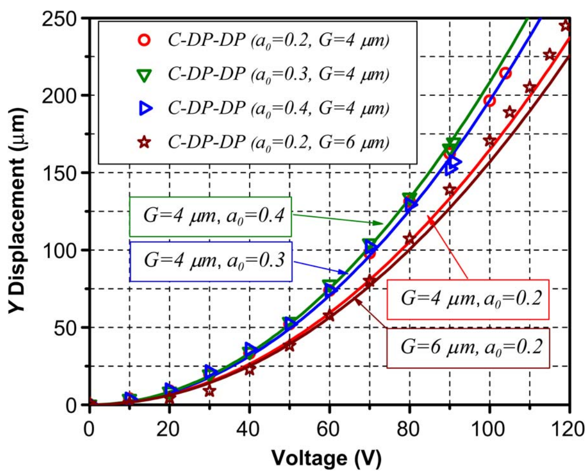

Fig. 15. Y displacement versus voltage for C-DP-DP flexure-based comb-drive actuators [*(solid lines) theoretical; (markers) experimental*].

stroke increases to 119 μm for a C-DP-DP flexure with the same dimensions as the previous DP-DP flexure. This stroke was further increased to 141 μm by using reinforced beams with $a_0 = 0.2$ while keeping all other dimensions the same. This stroke is 2.82 times higher than the DP-DP flexure, which highlights the superior performance of the reinforced C-DP-DP flexure compared with the traditional DP-DP flexure. In the last two cases, Table I indicates that $S = 1$ or 1.5 may not be an adequate stability margin when G is small (3 μm) and the actuation voltage is relatively large ($>$ 90 V). This is explained by (2), which shows that the critical stiffness in the presence of an error motion or misalignment E_x depends on the ratio E_x/G. For a smaller gap G, the effect of any misalignment is more pronounced, thereby necessitating a larger stability margin.

As previously shown, the stroke of a comb-drive actuator can be further improved by increasing the comb gap. This is demonstrated in Fig. 15, where a stroke of 215 μm was obtained using a C-DP-DP flexure with a beam length of 1 mm, a comb gap of 4 μm, and $a_0 = 0.2$. The benefit of beam reinforcement is also evident here. With an identical design, the experimentally measured strokes are 170 and 157 μm for $a_0 = 0.3$ and $a_0 = 0.4$, respectively. Finally, a large stroke of 245 μm at 120 V for a C-DP-DP flexure with a beam length of 1 mm, $a_0 = 0.2$, and a comb gap of 6 μm is also reported on this figure.

In the last four designs, given the larger comb gap, a stability margin of $S = 1$ or 1.5 appears to be adequate. In fact, an even smaller stability margin may be also considered because, in these cases, the experimentally measured stroke was limited due to a $\mathbf{Y}$-direction pull-in as opposed to the $\mathbf{X}$-direction snap-in considered in the design procedure.

In terms of the Y displacement versus actuation voltage, the theoretically predicted and experimental results for these seven cases agree within 4%, 31%, 11%, 18%, 6%, 4%, and 6%, in the order that they are presented above. Except for the one outlier (31%), these are within the expected range of deviation given the multiple sources of variability and uncertainty in dimensions and material properties in microfabricated devices.

D. Performance Comparison

While a direct comparison of the actuation stroke with previously reported comb-drive actuators is tricky because of the many variables (beam length, comb gap, maximum voltage, device footprint, etc.) and specific application-based constraints involved, we present a simple analytical basis that provides some level of comparison.

At large displacements, the first term in the square brackets in (21) is dominated by the second term. Therefore, if this first term is dropped, (21) can we rewritten as

$$Y_{\max}^3 = \left(\frac{\varepsilon}{E}\right)\left(\frac{6}{T_1^3}\cdot\sqrt{\frac{2}{\left(k_{11}^{(0)}\right)^3 g_{11}^{(1)}(1+S)}}\right)\left(NV_{\max}^2\right)\left(L_1^4\right). \tag{23}$$

Here, S is no longer assumed to be 1, as in (21); instead, it is retained as a function of the error motions E_x, as given in (3). The first term on the right-hand side above comprises physical constants, which remain invariant. The second term depends exclusively on the stiffness and error motion characteristics of the flexure mechanism used. The third term represents actuation effort and device footprint (due to N) and should therefore be minimized. The fourth term represents the overall device footprint and should be also minimized.

It can be separately shown that, for most flexure mechanisms based on the parallelogram module (e.g., P, DP-DP, and C-DP-DP) that are used in comb-drive actuation, a relation analogous to (23) can be derived. Everything else remains the same except the second term, which depends on the flexure mechanism design. This shows that, to achieve large stroke while minimizing actuation voltage and device footprint, this second term should be maximized via an appropriate flexure mechanism design. Therefore, a comparison between comb-drive actuators, which highlights the performance of the flexure mechanism used, can be conducted by plotting $Y_{\max}$ against $(NV_{\max}^2 L_1^4)^{1/3}$. This is done in Fig. 16, which illustrates the large stroke capability of the C-DP-DP flexure.

Another advantage of the proposed C-DP-DP flexure design is that, unlike the prebent DP-DP, it provides a K_x/K_y

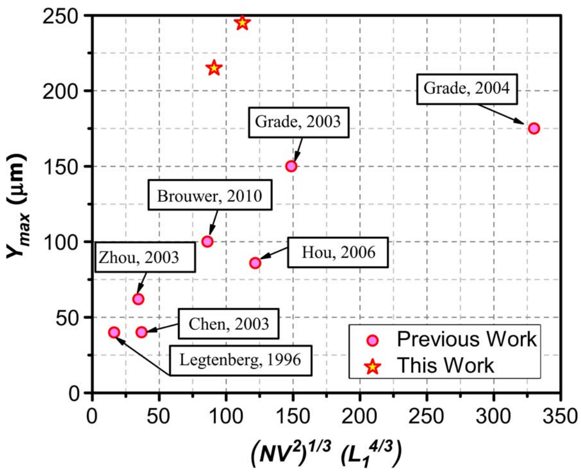

Fig. 16. Comparison of this paper's results with previously reported comb-drive actuator designs (V and L_1 are in volts and millimeters, respectively.) The top-left corner corresponds to large stroke, small device footprint, and small actuation voltage.

stiffness profile that is symmetric with respect to the $Y = 0$ displacement position. This allows bidirectional actuation and, therefore, twice the actuation stroke ($\sim 500\ \mu$m) for approximately the same device footprint and actuation voltage. For unidirectional operation, the stroke can be further improved by prebending the beams of a C-DP-DP flexure. Unlike the DP-DP case [see (13)], here, the maximum prebend limit is much higher while maintaining $S > 1$

$$Y_{P-B-\max} \approx \sqrt{\frac{4GL_1}{\sqrt{k_{11}^{(0)} g_{11}^{(1)}}}}. \tag{24}$$

For typical dimensions ($L_1 = 1$ mm, $G = 3\ \mu$m, $a_0 = 0.2$), this allowable prebend is as large as 400 μm, which in theory could lead to a Y displacement of approximately 500 μm at snap-in. Thus, ultimately, the flexure and the comb drive may be designed such that the actuation stroke is limited by the material failure criteria or the available actuation voltage, instead of sideways snap-in instability.

VI. Conclusion

There are four main contributions in this paper. Foremost, it has presented a novel C-DP-DP flexure mechanism with reinforced beams that offers high bearing and rotational direction stiffness (K_x and K_θ), low motion direction stiffness (K_y), and zero error motions (E_x and E_θ), all over a large range of motion direction displacement. Second, closed-form analytical expressions for these nonlinear stiffness characteristics have been provided that capture their parametric dependence on the flexure dimensions and the beam shape (a_0). Third, it has been shown that this flexure mechanism helps delay the onset of snap-in instability in comb-drive actuators to provide greater actuation stroke. A systematic step-by-step procedure for designing a C-DP-DP flexure-based comb-drive actuator to maximize its actuation stroke while minimizing device footprint and actuation voltage has been presented. Finally, several actuators have been microfabricated and experimentally tested to demonstrate very large actuation strokes. For 1-mm flexure beam length and 6-μm comb gap, a stroke of 245 μm is reported at 120 V. This experimental proof, along with the analytical formulation, clearly highlights the effectiveness of the C-DP-DP flexure for large-range comb-drive actuators. These results present the potential for eliminating sideways instability as the dominant effect that has so far limited the actuation stroke in electrostatic comb drives.

References

[1] W. C. Tang, T. C. H. Nguyen, and R. T. Howe, "Laterally driven polysilicon resonant microstructures," *Sens. Actuators*, vol. 20, no. 1/2, pp. 25–32, Nov. 1989.

[2] L. W. Lin, C. T. C. Nguyen, R. T. Howe, and A. P. Pisano, "Microelectromechanical filters for signal-processing," *Proc. IEEE Micro Electro Mech. Syst., Invest. Micro Struct., Sens., Actuators, Mach., Robot.*, pp. 226–231, 1992.

[3] K. Chang-Jin, A. P. Pisano, and R. S. Muller, "Overhung electrostatic microgripper," in *Proc. TRANSDUCERS*, 1991, pp. 610–613.

[4] D. M. Brouwer, B. R. de Jong, H. Soemers, and J. Van Dijk, "Sub-nanometer stable precision MEMS clamping mechanism maintaining clamp force unpowered for TEM application," *J. Micromech. Microeng.*, vol. 16, no. 6, pp. S7–S12, Jun. 2006.

[5] J. Dong and P. M. Ferreira, "Electrostatically actuated cantilever with SOI-MEMS parallel kinematic XY stage," *J. Microelectromech. Syst.*, vol. 18, no. 3, pp. 641–651, Jun. 2009.

[6] D. M. Brouwer, B. R. de Jong, and H. Soemers, "Design and modeling of a six DOFs MEMS-based precision manipulator," *Precis. Eng.*, vol. 34, no. 2, pp. 307–319, Apr. 2010.

[7] S. Awtar, A. H. Slocum, and E. Sevincer, "Characteristics of beam-based flexure modules," *J. Mech. Design*, vol. 129, no. 6, pp. 625–639, Jun. 2007.

[8] B. T. Chen and J. M. Miao, "Influence of deep RIE tolerances on comb-drive actuator performance," *J. Phys. D, Appl. Phys.*, vol. 40, no. 4, pp. 970–976, Feb. 21, 2007.

[9] K. Chen, A. Ayon, X. Zhang, and S. Spearing, "Effect of process parameters on the surface morphology and mechanical performance of silicon structures after deep reactive ion etching (DRIE)," *J. Microelectromech. Syst.*, vol. 11, no. 3, pp. 264–275, Jun. 2002.

[10] W. Huang and G. Y. Lu, "Analysis of lateral instability of in-plane comb drive MEMS actuators based on a two-dimensional model," *Sens. Actuators A, Phys.*, vol. 113, no. 1, pp. 78–85, Jun. 15, 2004.

[11] D. M. Brouwer, "Design principles for six degrees-of-freedom MEMS-based precision manipulators," Ph.D. dissertation, Univ. Twente, Enschede, The Netherlands, 2007.

[12] J. D. Grade, H. Jerman, and T. W. Kenny, "Design of large deflection electrostatic actuators," *J. Microelectromech. Syst.*, vol. 12, no. 3, pp. 335–343, Jun. 2003.

[13] R. Legtenberg, A. W. Groeneveld, and M. Elwenspoek, "Comb-drive actuators for large displacements," *J. Micromech. Microeng.*, vol. 6, no. 3, pp. 320–329, Sep. 1996.

[14] S. Awtar and T. Trutna, "An enhanced stability model for electrostatic comb-drive actuator design," in *Proc. ASME IDETC/CIE*, Montreal, QC, Canada, 2010, Paper 28943.

[15] E. Eleftheriou, T. Antonakopoulos, G. K. Binnig, G. Cherubini, M. Despont, A. Dholakia, U. Durig, M. A. Lantz, H. Pozidis, H. E. Rothuizen, and P. Vettiger, "Millipede—A MEMS-based scanning-probe data-storage system," *IEEE Trans. Magn.*, vol. 39, no. 2, pp. 938–945, Mar. 2003.

[16] J.-U. Park, M. Hardy, S. J. Kang, K. Barton, K. Adair, D. K. Mukhopadhyay, C. Y. Lee, M. S. Strano, A. G. Alleyne, J. G. Georgiadis, P. M. Ferreira, and J. A. Rogers, "High-resolution electrohydrodynamic jet printing," *Nat. Mater.*, vol. 6, no. 10, pp. 782–789, Oct. 2007.

[17] P. Beverly, G. Sivakumar, and T. Dallas, "Two-axis microstage system," *J. Microelectromech. Syst.*, vol. 17, no. 4, pp. 863–868, Aug. 2008.

[18] J. F. Domke, C. H. Rhee, Z. Liu, T. D. Wang, and K. R. Oldham, "Amplifying transmission and compact suspension for a low-profile, large-displacement piezoelectric actuator," *J. Micromech. Microeng.*, vol. 21, no. 6, pp. 067004-1–067004-8, Jun. 2011.

[19] J. Muthuswamy, M. Okandan, T. Jain, and A. Gilletti, "Electrostatic microactuators for precise positioning of neural microelectrodes," *IEEE Trans. Biomed. Eng.*, vol. 52, no. 10, pp. 1748–1755, Oct. 2005.

[20] B. P. van Drieenhuizen, N. I. Maluf, I. E. Opris, and G. T. A. Kovacs, "Force-balanced accelerometer with mG resolution, fabricated using silicon fusion bonding and deep reactive ion etching," in *Proc. TRANSDUCERS*, 1997, pp. 1229–1230.
[21] S. Awtar, K. Shimotsu, and S. Sen, "Elastic averaging in flexure mechanisms: A three-beam parallelogram flexure case study," *J. Mech. Robot.*, vol. 2, no. 4, pp. 041006-1–041006-12, Nov. 2010.
[22] J. D. Grade and H. Jerman, "Electrostatic microactuator with offset and/or inclined comb drive fingers," U.S. Patent 6 384 510, May 7, 2002.
[23] J. D. Grade, K. Y. Yasumura, and H. Jerman, "Advanced, vibration-resistant, comb-drive actuators for use in a tunable laser source," *Sens. Actuators A, Phys.*, vol. 114, no. 2/3, pp. 413–422, Sep. 2004.
[24] K. H. L. Chau, S. R. Lewis, Y. Zhao, R. T. Howe, S. F. Bart, and R. G. Marcheselli, "An integrated force-balanced capacitive accelerometer for low-g applications," *Sens. Actuators A, Phys.*, vol. 54, no. 1–3, pp. 472–476, Jun. 1996.
[25] H. Jerman, J. D. Grade, and J. D. Drake, "Electrostatic microactuator and method for use thereof," U.S. Patent 5 998 906, Dec. 7, 1999.
[26] G. Y. Zhou and P. Dowd, "Tilted folded-beam suspension for extending the stable travel range of comb-drive actuators," *J. Micromech. Microeng.*, vol. 13, no. 2, pp. 178–183, Mar. 2003.
[27] R. V. Jones, *Instruments and Experiences: Papers on Measurement and Instrument Design*. New York: Wiley, 1988.
[28] D. M. Brouwer, A. Otten, J. B. C. Engelen, B. Krijnen, and H. M. J. R. Soemers, "Long-range elastic guidance mechanisms for electrostatic comb-drive actuators," in *Proc. EUSPEN Int. Conf.*, Delft, The Netherlands, 2010, vol. 1, pp. 462–465.
[29] W. J. Ye, S. Mukherjee, and N. C. MacDonald, "Optimal shape design of an electrostatic comb drive in microelectromechanical systems," *J. Microelectromech. Syst.*, vol. 7, no. 1, pp. 16–26, Mar. 1998.
[30] B. D. Jensen, S. Mutlu, S. Miller, K. Kurabayashi, and J. J. Allen, "Shaped comb fingers for tailored electromechanical restoring force," *J. Microelectromech. Syst.*, vol. 12, no. 3, pp. 373–383, Jun. 2003.
[31] M. T. K. Hou, G. K. W. Huang, J. Y. Huang, K. M. Liao, R. S. Chen, and J. L. A. Yeh, "Extending displacements of comb drive actuators by adding secondary comb electrodes," *J. Micromech. Microeng.*, vol. 16, no. 4, pp. 684–691, Apr. 2006.
[32] J. C. Chiou, Y. J. Lin, and C. F. Kuo, "Extending the traveling range with a cascade electrostatic comb-drive actuator," *J. Micromech. Microeng.*, vol. 18, no. 1, pp. 015018-1–015018-7, Jan. 2008.
[33] S. Kota, J. Hetrick, Z. Li, and L. Saggere, "Tailoring unconventional actuators using compliant transmissions: Design methods and applications," *IEEE/ASME Trans. Mechatronics*, vol. 4, no. 4, pp. 396–408, Dec. 1999.
[34] S. Kota, J. Joo, Z. Li, S. M. Rodgers, and J. Sniegowski, "Design of compliant mechanisms: Applications to MEMS," *J. Analog Integr. Circuits Signal Process.*, vol. 29, no. 1/2, pp. 7–15, Nov. 2001.
[35] X. T. Huang, M. T. Saif, and N. C. MacDonald, "A micromotion amplifier," in *Proc. IEEE 9th Annu. Int. Workshop Micro Electro Mech. Syst., Invest. Micro Struct., Sens., Actuators, Mach., Syst.*, 1996, pp. 424–428.
[36] Y. Nada, M. Medhat, M. Nagi, F. Marty, B. Saadany, and T. Bourouina, "Mechanical displacement multiplier: 250 μm stable travel range MEMS actuator using frictionless simple compliant structures," in *Proc. IEEE 25th Int. Conf. MEMS*, 2012, pp. 1161–1164.
[37] M. Olfatnia, S. Sood, and S. Awtar, "Large stroke electrostatic comb-drive actuators based on a novel flexure mechanism," in *Proc. Hilton Head Solid-State Sens., Actuators, Microsyst. Workshop*, 2012, pp. 409–412.
[38] S. Sood, *Single-Axis Flexure Mechanisms Approaching Ideal Bearing Characteristics*. Ann Arbor, MI: Univ. Michigan Press, 2012.
[39] J. L. A. Yeh, C. Y. Hui, and N. C. Tien, "Electrostatic model for an asymmetric combdrive," *J. Microelectromech. Syst.*, vol. 9, no. 1, pp. 126–135, Mar. 2000.
[40] D. Elata and V. Leus, "How slender can comb-drive fingers be?" *J. Micromech. Microeng.*, vol. 15, no. 5, pp. 1055–1059, May 2005.
[41] M. A. Hopcroft, W. D. Nix, and T. W. Kenny, "What is the Young's modulus of silicon?" *J. Microelectromech. Syst.*, vol. 19, no. 2, pp. 229–238, Apr. 2010.
[42] N. Tas, T. Sonnenberg, H. Jansen, R. Legtenberg, and M. Elwenspoek, "Stiction in surface micromachining," *J. Micromech. Microeng.*, vol. 6, no. 4, pp. 385–397, Dec. 1996.

Mohammad Olfatnia received the B.S. and M.S. degrees in applied mechanics from Isfahan University of Technology, Isfahan, Iran, in 2005 and 2007, respectively, and the Ph.D. degree from Nanyang Technological University, Singapore, in 2011.

He is currently a Research Fellow with the Precision Systems Design Laboratory, Department of Mechanical Engineering, University of Michigan, Ann Arbor. His research interests include the design and fabrication of MEMS-based sensors and actuators and mechatronics systems, and extending their performance limits via model-based multidomain design.

Siddharth Sood received the B.Tech. degree in mechanical engineering from the Indian Institute of Technology, Kanpur, India, in 2010. He is currently working toward the M.S. degree in the Precision Systems Design Laboratory, University of Michigan, Ann Arbor. His Master's thesis work is on developing analysis and validation tools for flexure bearings. It also encompasses a holistic design procedure for comb drive actuators employing flexure bearings and metrics to compare the performance of different flexure designs.

He is also currently with the Intelligent Systems Division, National Institute of Standards and Technology (NIST), Gaithersburg, MD, as a Guest Researcher. At NIST, he is currently working on developing a MEMS test bed to characterize the speed and resolution of atomic force microscopes and quantify them for comparison across different instruments.

Jason J. Gorman (M'02) received the B.S. degree in aerospace engineering from Boston University, Boston, MA, in 1994 and the M.S. and Ph.D. degrees in mechanical engineering from The Pennsylvania State University in 1999 and 2002, respectively.

In 2002, he joined the National Institute of Standards and Technology (NIST), Gaithersburg, MD, as an NRC Postdoctoral Research Associate and has since become a member of the technical staff with the Intelligent Systems Division, where he leads the NEMS Measurement Science project. His research interests include micro- and nanoelectromechanical systems, scanning probe microscopy, nanomanufacturing, precision measurements, dynamic systems, and robust and nonlinear control.

Shorya Awtar received the B.Tech. degree from the Indian Institute of Technology Kanpur, Kanpur, India, in 1998, the M.S. degree from Rensselaer Polytechnic Institute, Troy, NY, in 2000, and the Sc.D. degree from Massachusetts Institute of Technology, Cambridge, in 2003, all in mechanical engineering.

Prior to joining the University of Michigan, Ann Arbor, he worked at the General Electric Company Global Research Center until 2006. He is currently an Assistant Professor of Mechanical Engineering and the Director of the Precision Systems Design Laboratory at the University of Michigan. His engineering and research interests include machine design, flexure mechanisms, precision engineering, and mechatronic systems. The current focus of his research group is on precision motion systems for nanometrology and nanomanufacturing, minimally invasive surgical tools, and microscale motion stages.

Dr. Awtar is a member of the American Society of Mechanical Engineers (ASME). He was a recipient of the National Science Foundation CAREER Award in 2009 and the ASME Leonardo da Vinci Award in 2011.